DOI: 10.1002/cphc.201100486

Thermal Breakdown of ZnTe Nanowires

Keivan Davami,[a] Hessam M. Ghassemi,[b] Reza S. Yassar,[b] Jeong-Soo Lee,*[a] and M. Meyyappan*[a, c]

As the applications for inorganic nanowires continuously grow, studies on the stability of these structures under high electrical/thermal stress conditions are needed. ZnTe nanowires are grown by the vapor-liquid-solid technique and their breakdown under Joule heating is studied through in situ monitoring in a transmission electron microscope (TEM). The experimental setup, consisting of a scanning tunneling microscope (STM) and a movable piezotube inside the TEM, allows the manipulation of a single nanowire. A voltage applied to the STM tip in contact with a ZnTe nanowire leads to the breakdown of the nanowire into Zn and Te particles or balls which is observed in real time. These balls grow by Ostwald ripening, rendering the surface morphology of the ZnTe nanowire progressively rough. Diffraction patterns along the stem of the wire after the partial breakdown showed substantially smaller lattice spacing compared to 0.35 nm for pristine ZnTe nanowires.

1. Introduction

Inorganic nanowires have received considerable attention due to their interesting properties, quantum confinement and large surface-to-volume ratio.[1] Among them, II-VI wide bandgap semiconductors such as ZnTe, CdTe and others received attention as attractive candidates for optoelectronic devices, solar cells, detectors, and thermoelectric devices.[1,2] ZnTe is a semiconductor with a direct gap of 2.2 eV at 300 K and a Bohr radius of 6.2 nm. When the nanowire diameter is below 50 nm, a relatively strong quantum confinement with a marked blue shift was seen for ZnTe nanowires.[3] The applications mentioned above demand nanowires of uniform diameter and controllable morphology. The vapor-liquid-solid (VLS) technique is a popular method of choice to grow these nanowires[4–10] since it provides nanowires with exceptional surface quality, controllable dimensions, and other features coveted in device fabrication. As a chemical vapor deposition process, the VLS technique is also amenable for the growth on patterned substrates and suitable for integration as a step in the device processing sequence. In the case of ZnTe, widely varying structures ranging from cylindrical to tapered nanowires and nanoribbons were obtained depending on growth, temperature and other process parameters.[7,10] Nevertheless, a narrow temperature window was shown to yield nearly uniform diameter nanowires.[10]

Applications in electronics, detectors, thermoelectric and other devices require the electrical characterization and investigation of the thermal stability under high applied currents. For example, phase-change nanowires such as $Ge_2Sb_2Te_5$ were shown to suffer from phase segregation due to Joule heating under high current densities,[11] which is a critical issue in the development of nanowire-based random access memory. The high electrical and thermal stress experienced during the operation was shown to lead to the movement of Sb and Ge toward the cathode and of Te toward the anode in phase-change nanowire memory devices. A destructive breakdown in individual GaN nanowires was observed at about 1000 K due to Joule heating with failure occurring through thermal decomposition.[12] The understanding of such limitations in nitride nanowires is important for the development of their applications, such as in light emitting diodes and high electron mobility transistors. Besides inducing damages, Joule heating can also be utilized to weld materials, such as the ends of two adjacent Pt nanowires in an effort to manipulate nanostructures.[13] To the best of the authors knowledge, current-induced breakdown of II-VI materials has not been reported yet and the work presented herein provides results from stability studies using in situ transmission electron microscopy (TEM) for the characterization of ZnTe nanowires. An experimental setup consisting of a scanning tunneling microscope (STM) and a movable piezotube inside the TEM (Figure 1) allowed the manipulation of a single ZnTe nanowire and the application of a voltage to the STM tip led to the breakdown of the nanowire into Zn and Te balls observed in real time.

2. Results and Discussion

The ZnTe nanowires are 20–150 nm in diameter and 100 nm to several microns long as shown in the scanning electron microscopy (SEM) images in Figure 2. Based on a previous parametric optimization study,[10] only conditions that yield nano-

[a] K. Davami, Prof. J.-S. Lee, Dr. M. Meyyappan
Division of IT-Convergence Engineering
Pohang University of Science and Technology, Pohang (Korea)
E-mail: m.meyyappan@nasa.gov
ljs6951@postech.ac.kr

[b] H. M. Ghassemi, Prof. R. S. Yassar
Dept. of Mechanical Engineering
Michigan Technological University, Houghton, MI 49931 (USA)

[c] Dr. M. Meyyappan
NASA Ames Research Center
Moffett Field, CA 94035 (USA)

Supporting information for this article is available on the WWW under http://dx.doi.org/10.1002/cphc.201100451.

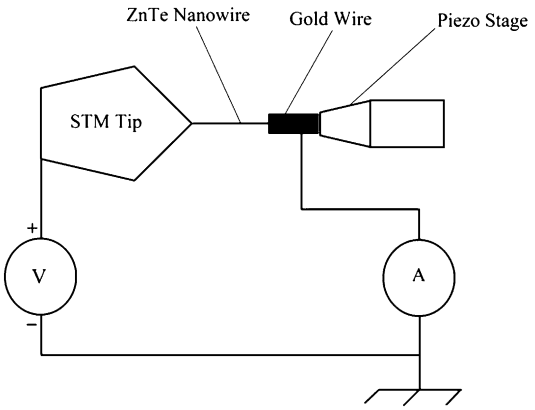

Figure 1. STM-TEM setup. An individual ZnTe nanowire is placed between the STM tip and a gold wire. The gold wire with the attached nanowire is placed on a moveable piezotube enabling 3D motion toward the STM probe.

wires were chosen to exclude tapered structures and nanoribbons. EDX results confirm stoichiometries close to 1:1 for Zn and Te. High resolution TEM analysis and electron diffraction patterns obtained for various nanowires show a lattice spacing of 0.35 nm, corresponding to the d-spacing of the (111) plane of ZnTe face centered cubic (fcc) structure.[10] Figure 3 shows Raman spectra taken for three representative ZnTe nanowire samples which provide the characteristic longitudinal optical mode (LO) at 204 cm^{-1}. Strong overtones of 2 LO, 3 LO and 4 LO (410.0, 615.3 and 821.9 nm respectively) are observed because of the resonant excitation energy at 2.26 eV and the high density of nanowire phonon states at the resonant excitation.[14] The high quality of the crystalline nanostructure is confirmed by the narrow full width half maximum (FWHM) bands of the LO and its overtones. Aggregates of Te were detected in very small amounts (around 120 cm^{-1}) in only one sample out of three (Figure 3). This observation differs from other growth reports indicating the presence of Te aggregates.[5,15] It is believed that these Te aggregates form in layer structures or on the surface of nanowires where they can be detected by Raman analysis in small quantities.[7,15] The absence of Te peaks in our Raman data indicates that the ZnTe nanowire samples are uniform rather than layered, and the high quality of crystalline structures contain negligible surface states for Te aggregates to reside. Finally, since the radii of these nanowires are far larger than the Bohr radius, no quantum confinement effects are expected and the observed peaks are the same as those for the crystalline ZnTe thin film.

The TEM analysis revealed the presence of an amorphous native oxide layer on the surface of certain nanowires which, in some cases, reaches a thickness of up to 5 nm (Figure 4). Such layers have also been noticed by Kirmse et al.[6] and shown to be ZnO, which has had to be formed after the growth since there was no possibility for the presence of oxygen in their molecular beam epitaxy approach. While post-growth formation of ZnO layer is a possibility in our case, its formation in the growth chamber may not be entirely ruled out under moderate vacuum growth conditions applied during

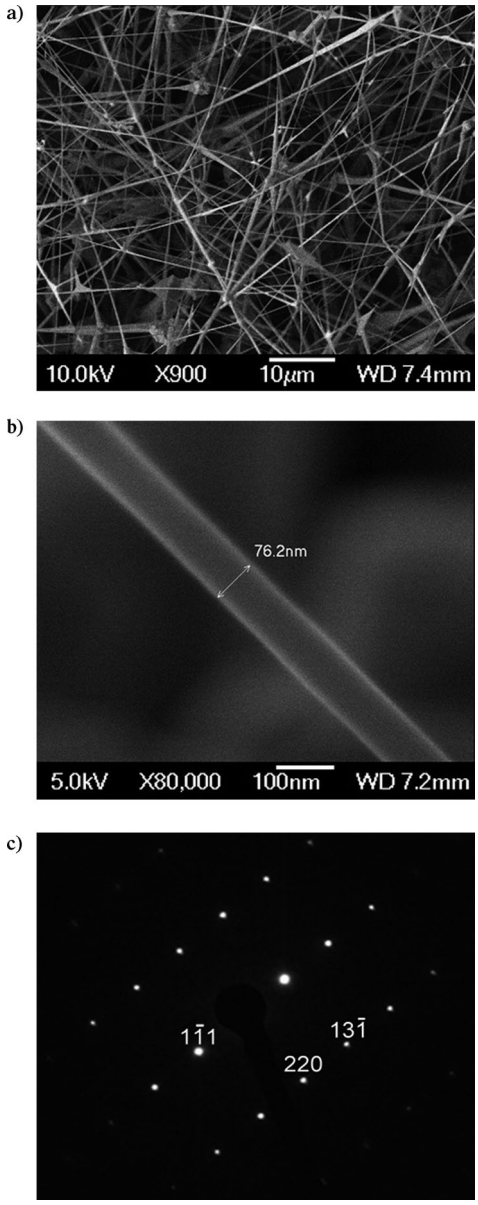

Figure 2. SEM images of a) a mat of ZnTe nanowires and b) an individual nanowire ~70 nm in diameter. c) SAED pattern of a grown ZnTe nanowire.

the VLS process. No Raman modes assignable to ZnO[16–18] are visible in Figure 3, possibly because the available excitation energy (2.3 eV) in Raman measurements is 1.0 eV below the ZnO bandgap (3.3 eV), used with a low power of 0.2 mW herein. The Raman signatures of thin ZnO layers are unlikely to be detectable under such non-resonant, low power Raman measurement conditions. In any case, the presence of an oxide layer affects the resistivity of the nanowires and must be removed prior to the conducting of thermal stability studies.

Typically, the oxide layer is removed by etching the samples in an HF solution. In the TEM-STM setup herein, however, two alternative methods were pursued. In the first method, a nanowire was welded to the STM tip and then pulled back and broken. The oxide layer at the end of the nanowire was left attached to the STM tip. The nanowire itself was then moved

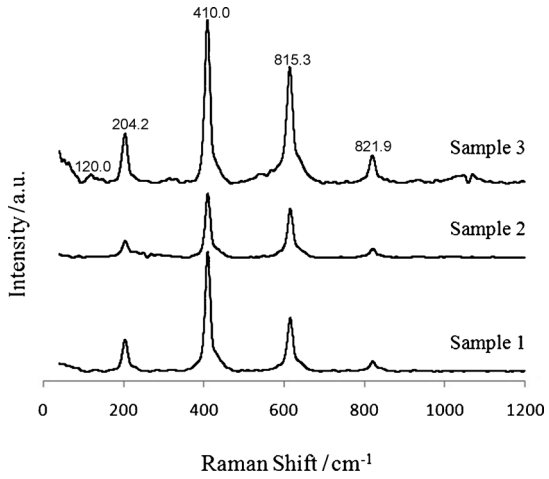

Figure 3. Raman spectra of three representative ZnTe samples. Growth conditions are identical to those described in the text except that Samples 1 and 2 were grown with flow rates of 150 sccm and 60 sccm. Sample 3 was synthesized with 900 °C as source evaporation temperature.

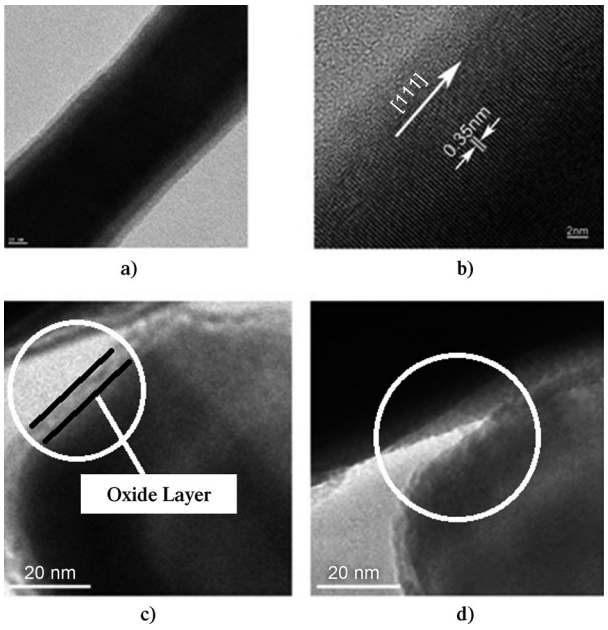

Figure 4. a, b) TEM images showing a thin oxide layer on the nanowire. The lattice spacing is 0.35 nm for the grown ZnTe nanowire and growth is along $<111>$ direction. Scale bars are 10 nm and 2 nm. c, d) Removal of the oxide layer with an STM bias of -10 V (nanowire diameter = 70 nm). The bias-induced heating removes the oxide layer near the tip (area is marked by the circle).

and connected to another spot on the STM tip and the resistivity was measured. In the second method, after bringing the nanowire in contact with the STM tip, a current was passed through the nanowire for a short period of time (which depended on the diameter and always less than 10 min), with a bias voltage of -10 V. This increases the temperature in the vicinity of the contact area enough to remove the oxide layer (Figure 4). Interestingly, longer exposure times led to the decomposition of the nanowire itself, as is discussed later. The second method is preferable since it does not break the nanowire. The current-voltage data for a nanowire of 100 nm diameter and 4 μm in length shows a resistivity of 2791 Ω cm which is nearly an order of magnitude lower than for that with an intact oxide layer.

Next, decomposition under Joule heating is discussed using a ZnTe nanowire of 100 nm in diameter and 200 nm in length as a representative case study. In this experiment the STM probe was fixed, while the gold wire with the nanowire was moved in three dimensions. The entire process was monitored in real time by TEM imaging and a movie of the whole process was recorded (available in the Supplementary Information). Applying a 10 V bias to the STM tip (after oxide removal) and holding it constant for 5 min caused the temperature to rise due to Joule heating. After 4 min, formation of Zn and Te particles or balls was observed shown in Figure 5 a and Figure 5 b. The balls started growing further with time and in Figure 5 c and Figure 5 d, the Zn and Te balls can be distinguished by their color, grey and black, respectively. The higher contrast of the particles can be explained by strain fields associated with

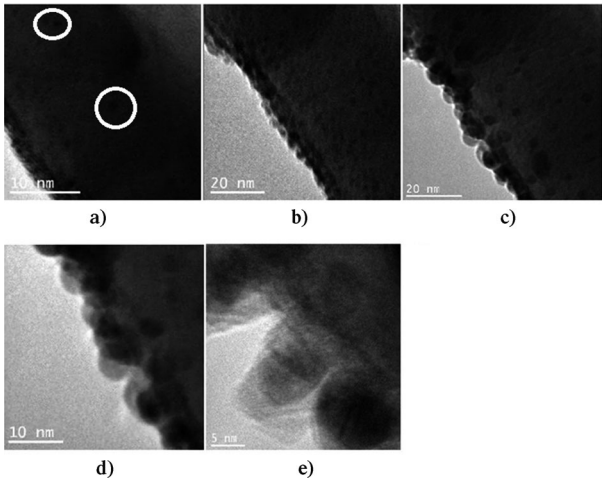

Figure 5. TEM images showing the decomposition of a ZnTe nanowire (d = 100 nm, L = 200 nm) with a 10 V bias. a) Onset of decomposition at 240 s; b) after 280 s; c) and d) growth of Zn and Te balls (grey and black) after 480 s; and e) surface of the nanowire after the evaporation of Zn and Te balls. The circles highlight the presence of the balls. The video of this process is available in the Supplementary Information.

their segregation and formation. The growth of these particles can be attributed to Ostwald ripening, wherein the small crystals formed initially disappear slowly except for a few that grow larger at the expense of smaller ones. After precipitation and evaporation of the balls a rough surface remained on the nanowire (Figure 5 e).

Case studies involving several other nanowires of different diameters and lengths and those with an intact gold catalyst particle at the tip (a consequence of the VLS growth) agree on the observations made above. Figure 6 shows a nanowire of 58.4 nm in diameter and a length of 450 nm with a gold catalyst particle at the tip before and 20 min after the onset of de-

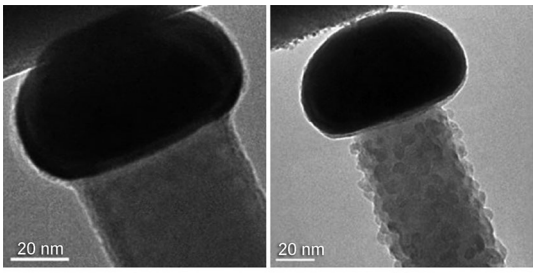

Figure 6. ZnTe nanowire with an intact gold catalyst particle at the tip. a) Before decomposition and b) 20 min after the onset of decomposition. The diameter in (a) is uniformly 58.4 nm, whereas in (b) the diameter differs along the stem with an average of 53.0 nm.

composition. After 20 min, the nanowire exhibits a rough surface with a reduction in diameter (53 nm on average across the length of the nanowire). Several shots of the movie during decomposition of this wire are shown in Figure 7. The corresponding probe bias was 30 V. Formation and growth of the balls by Ostwald ripening are evident and while the larger crystals grow, the areas around them are depleted of smaller crystals. However, the gold particle has not melted but is left intact at the tip even at this stage, maintaining its shape and size, as seen in Figure 6b.

We do not have an estimate of the current density during decomposition as the current is unstable during heating. While the resistivity is rather high at the first application of the bias (~1216 ohm cm), we believe that it drastically decreases with an increase in current as the process continues. Observations of an increase in conductivity and a jump in the current have been reported by Hummelgård et al.[19] for bundles of $Mo_6S_3I_6$ nanowires experiencing Joule heating. A breakdown in Joule-heated GaN nanowires has been reported by Westover et al.,[12] wherein 0.2–0.67 μm thick individual nanowires, laid on a silicon wafer, have been subjected to high current densities (in contrast to an individual suspended nanowire as shown in the setup in Figure 1). The decomposition in that case has been triggered by the formation of Ga balls, leading eventually to a breakdown. Four-point probe measurements have provided an estimate of 3×10^6 A cm^{-2} for the average current density, damaging the GaN nanowires. The breakdown of SiC nanowires,[20] in contrast to ZnTe and GaN, occurs through the evaporation of core silicon carbide after removal of the surface oxide.

Since our STM-TEM setup did not have an in situ temperature measurement capability, we were not able to obtain the temperature for the onset of decomposition. Instead, a finite element simulation involving a coupled thermal and electrical analysis of the tungsten STM tip-nanowire-gold wire (Figure 1) was used to estimate the temperature at 4 min (onset of decomposition in Figure 5) to 832 °C. The simulation, performed with ANSYS software, included 1D heat conduction along the nanowire, Joule heating due to the applied bias at the STM tip, radiation loss, and heat dissipation through the gold wire which was treated as a boundary condition. Convective losses were assumed to be negligible under vacuum conditions. This estimate is only an approximation since accurate resistivity during the heating was not available for input to the simulation. The gold particle of the size in Figure 6 (~65 nm) melts at around 1000 °C[21] and the bulk melting temperatures of Zn and Te are 419.53 °C and 449.51 °C, respectively. These temperatures mark the upper and lower limits for the decomposition of the ZnTe nanowire, thus the finite element simulation result of 832 °C appears to be a reasonable estimate.

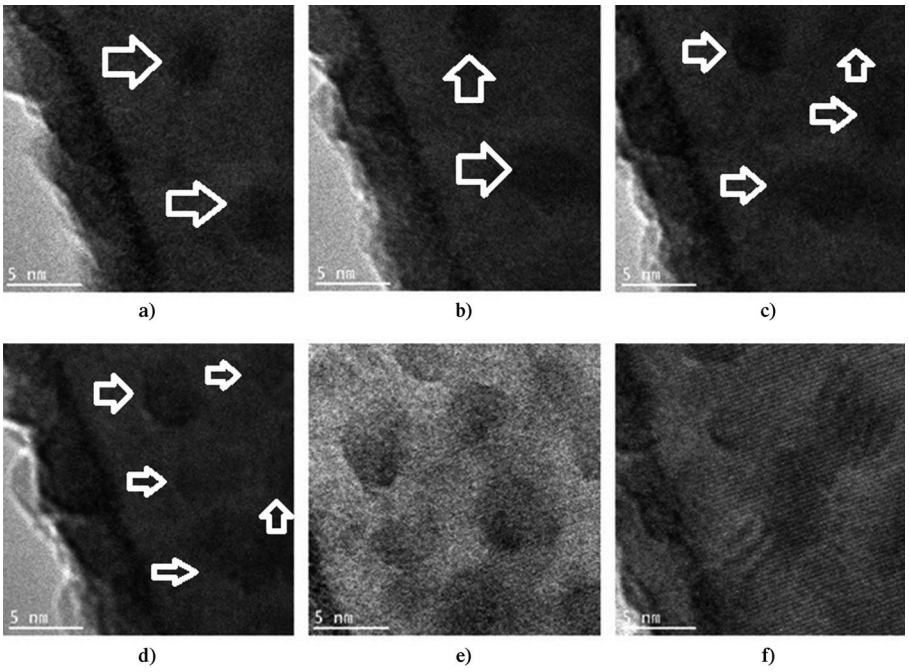

Figure 7. Zn and Te ball formation during the breakdown of the ZnTe nanowire shown in Figure 6. Because of the high magnification, the gold particle is not seen and only a portion of the nanowire is shown. a) After 5 min; b) after 7 min; c) after 8 min; d) after 11 min; e) after 15 min.; and f) after 20 min. The balls grow and aggregate. The arrows point towards the balls.

The electron diffraction pattern of the nanowire confirms the decomposition as well (Figure 8). The circular pattern indicates the presence of micrograins at this stage, in contrast to the regular spot pattern (Figure 2) characteristic for the perfect single crystalline nanowire before the decomposition.[10] It is well known that the lattice spacing in the ZnTe nanowire is 0.35 nm[4,7,10] and the measured spacing before decomposition agrees with this value. After decomposition, the lattice spacing was measured at different spots, indicated in Figure 8. It was 0.22 nm in the

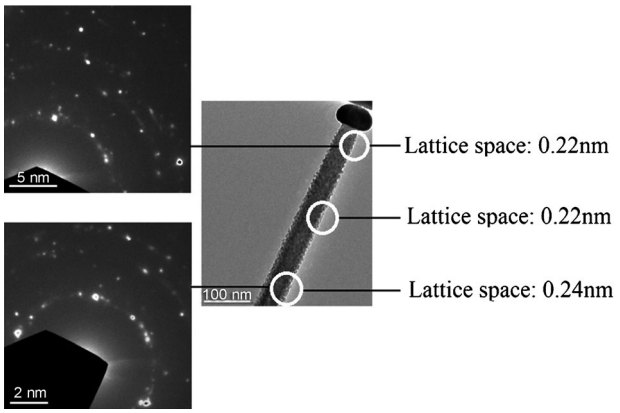

Figure 8. Lattice spacing and diffraction patterns at different spots on the nanowire.

region close to the gold particle and 0.24 nm at the other end. The lattice constants for Zn and Te are 0.266 nm and 0.445 nm respectively. It is hard to draw any conclusions about the local composition from the observed spacings in Figure 8 since these values are single measurements in three different locations. The lattice spacing could vary across the radial cross section in each of those locations corresponding to the local presence of Zn and Te balls, as well as intact ZnTe. It would have been elucidating to conduct Raman analysis on the wire shown in Figure 8 to look for modes assignable to Te and Zn clusters, but the recovery of a single nanowire from the setup in Figure 1 was not feasible. Interestingly if heating leads to melting the diffraction pattern would then disappear. Indeed, this transition can be used to measure the melting points of individual nanowires as shown for phase change materials, such as GeTe and In_2Se_3.[22,23]

3. Conclusions

As nanowires continue to attract attention for electronics, optoelectronics, detectors, thermoelectric devices and other applications involving high current and power densities on nanoscale, it is important to understand the stability of these nanostructures. Herein, using ZnTe nanowire as a case study, we investigated and monitored the breakdown of nanowires under an applied bias in situ in a TEM. Joule heating led to the decomposition of the nanowires into their constituent elements, which appear in the form of tiny balls and grow due to Ostwald ripening. A finite element simulation of the thermal and electrical transport provides an estimation of the decomposition temperature.

Experimental

ZnTe nanowires were grown in a two-zone furnace VLS growth reactor (2.54 cm quartz tube) with high purity ZnTe powder (99.99%, Sigma-Aldrich, 0.1 g) as the source material.[10] It was heated to 850 °C upstream in a quartz boat and the vapor was carried by 30 sccm of carrier gas (5:1 molar ratio argon:hydrogen) downstream to the growth zone containing small pieces of silicon wafers, sputtered with a 1–3 nm gold layer. The growth zone temperature was maintained at 600 °C. The temperature ramp in both zones was 15° min^{-1} at a pressure of 300 Torr. After 90 min, the reactor was cooled to room temperature under an argon flow prior to the removal of the wafers. The nanowires were characterized by scanning electron microscopy (JEOL JSM-7401F), high resolution TEM (JEOL JEM-2200FS) energy dispersive X-ray spectroscopy (EDX), and Raman spectroscopy (Bruker optics, Senterra, 532 nm He laser at 0.2 mW power).

The current-voltage measurements and in situ monitoring of Joule-heating effects were performed in a TEM equipped with a STM as shown in Figure 1 (JEOL JEM-4000FX operating at 200 kV). The surface of the silicon substrate with the nanowires was scratched with a gold wire, resulting in the attachment of a ZnTe nanowire to the gold wire due to van der Waals forces. The gold wire was placed on a manipulator with a piezotube which allowed the three dimensional motion towards the STM. The tip of the STM probe was brought in contact with the ZnTe nanowire and a constant voltage was applied to the STM tip while monitoring the changes in morphology using the TEM.

Acknowledgements

This work was supported by the World Class University program through the National Research Foundation of Korea funded by the Ministry of Education, Science and Technology under Project R31-10100. Part of this work was done at MTU during KD's visit and Professor Yassar's group is acknowledged for hosting the visit. RSY would like to acknowledge the funding support through the NSF-DMR Grant 0820884 and NSF-CMMI Grant 0926819. Dr. Bin Chen is acknowledged for her insightful comments on the Raman analysis.

Keywords: nanowires · surface analysis · thermal breakdown · thermal stress · thermoelectrics

[1] M. Meyyappan, M. K. Sunkara, *Inorganic Nanowires: Applications, Properties and Characterization*, CRC Press, Boca Raton, FL, **2010**.
[2] N. Mingo, *Appl. Phys. Lett.* **2004**, *85*, 5986–5988.
[3] L. Li, Y. Yang, X. Huang, G. Li, L. Zhang, *J. Phys. Chem. B* **2005**, *109*, 12394–12398.
[4] H. B. Huo, L. Dai, C. Liu, L. P. You, W. Q. Wang, R. M. Ma, G. Z. Ran, G. G. Qin, *Nanotechnology* **2006**, *17*, 5912–5915.
[5] E. Janik, P. Dluzewski, S. Kret, A. Presz, H. Kirmse, W. Neumann, W. Zaleszczyk, L. T. Baczewki, A. Petroutchik, E. Dynowka, J. Sadowski, W. Calibe, G. Karczewski, T. Wojtowicz, *Nanotechnology* **2007**, *18*, 475606.
[6] H. Kirmse, W. Neumann, S. Kret, P. Dluzewski, E. Janik, G. Karczewski, T. Wojtowicz, *Phys. Status Solidi C* **2008**, *5*, 3780–3784.
[7] Q. F. Meng, C. Jiang, S. X. Mao, *J. Cryst. Growth* **2008**, *310*, 4481–4486.
[8] Q. F. Meng, C. B. Jiang, and S. X. Mao, *Appl. Phys. Lett.* **2009**, *94*, 043111.
[9] S. Li, Y. Jiang, D. Wu, L. Wang, H. Zhong, B. Wu, X. Lan, Y. Yu, Z. Wang, J. Jie, *J. Phys. Chem. C* **2010**, *114*, 7980–7985.
[10] K. Devami, D. Kang, J. S. Lee, M. Meyyappan, *Chem. Phys. Lett.* **2011**, *504*, 62–66.
[11] C. Kim, D. Kang, T. Y. Lee, K. H. P. Kim, Y. S. Kang, J. Lee, S. W. Nam, K. B. Kim and Y. Kang, *Appl. Phys. Lett.* **2009**, *94*, 193504.
[12] T. Westover, R. Jones, J. Y. Huang, G. Wang, E. Lai, A. A. Talin, *Nano Lett.* **2009**, *9*, 257–263.
[13] H. Tohmyoh, T. Imaizumi, H. Hayashi, M. Saka, *Scr. Mater.* **2007**, *57*, 953–956.
[14] H. B. Huo, L. Dai, D. Y. Xia, G. Z. Ran, L. P. You, B. R. Zhang, G. G. Qin, *J. Nanosci. Nanotechnol.* **2006**, *6*, 1182–1184.

[15] W. Szuszkiewicz, J. F. Morhange, E. Dynowska, E. Janik, W. Zalesczyk, A. Presz, G. Karczewski, T. Wojtowicz, *J. Phys. Cont. Series* **2007**, *92*, 012040.
[16] J. B. Cui, C. P. Daghlian, U. J. Gibson, R. Pusche, P. Geithner, L. Ley, *J. Appl. Phys.* **2005**, *97*, 044315.
[17] C. Xu, K. Rho, J. Chun, D. E. Kim, *Appl. Phys. Lett.* **2005**, *87*, 253104.
[18] H. T. Ng, B. Chen, J. Li, J. Han, M. Meyyappan, J. Wu, S. X. Li, E. Haller, *Appl. Phys. Lett.* **2003**, *82*, 2023 – 2025.
[19] M. Hummelgård, R. Zhang, T. Carlberg, D. Vengust, D. Dvorsek, D. Mihailovic, H. Olin, *Nanotechnology* **2010**, *21*, 165704.
[20] H. Kohno, Y. Mori, S. Takeda, Y. Ohno, I. Yonenaga, S. Ichikawa, *Appl. Phys. Express* **2010**, *3*, 055001.
[21] Ph. Buffat, J. P. Borel, *Phys. Rev. A* **1976**, *13*, 2287 – 2298.
[22] X. Sun, B. Yu, G. Ng, M. Meyyappan, *J. Phys. Chem. C* **2007**, *111*, 2421 – 2425.
[23] X. Sun, B. Yu, G. Ng, T. D. Nguyen, M. Meyyappan, *Appl. Phys. Lett.* **2006**, *89*, 233121.

Received: June 23, 2011
Revised: October 23, 2011
Published online on November 30, 2011

